Morphological Impact of Segment Dispersity in Lithium Salt-Doped Poly(styrene)/Poly(ethylene oxide) Triblock Polymers

Hongyun Xu,† Eric M. Greve§,¶ and Mahesh K. Mahanthappa†,*

† *Department of Chemical Engineering & Materials Science, University of Minnesota, 421 Washington Ave. S.E., Minneapolis, MN 55455*

§ *Department of Chemistry, University of Wisconsin–Madison, 1101 University Ave., Madison, WI 53706*

¶ *Present address: Department of Chemistry, Marquette University, Milwaukee, WI 53233*

* *Corresponding author: maheshkm@umn.edu; +1 (612) 625-4599*

Abstract

We investigate the impact of center segment dispersity on the phase behavior of 17 lithium salt-doped poly(styrene-*block*-oligo(ethylene oxide) carbonate-*block* styrene) (bSOS) triblock polymers, in which broad dispersity O blocks ($Đ_O = M_w/M_n \approx 1.45$) are situated between narrow dispersity S segments ($Đ_S \leq 1.18$) with volume fractions $f_O = 0.33–0.69$ and total $M_n = 11.6–43.8$ kg/mol. Broad dispersity bSOS triblocks are synthesized by a tandem polycondensation and atom transfer radical polymerization (ATRP) reaction sequence. Using temperature-dependent small-angle X-ray scattering (SAXS), we map the morphology diagrams for bSOS samples variously doped with lithium bis(trifluoromethylsulfonyl)imide (LiTFSI) with r = (mol Li^+)/(mol ethylene oxide) = 0.00–0.09. As compared to the phase behavior exhibited by 13 LiTFSI-doped, narrow dispersity SOS triblocks (nSOS) with $f_O = 0.30–0.58$ and $M_n = 7.1–45.2$ kg/mol, we demonstrate that O segment dispersity shifts the lamellar morphology window to higher $f_{O/salt}$ and the lamellar microdomains dilate at each r-value. The critical segregation strength for microphase separation is calculated to be $(\chi N/2)_{ODT} = 10.3–11.1$ for $r = 0.01–0.05$ as compared to the mean-field theory prediction $(\chi N/2)_{ODT} = 8.95$. These findings are interpreted in terms of a competition between amplified monomer concentration fluctuations due to O segment dispersity in these high χ/low N triblocks and ordered morphology stabilization due to preferential lithium salt solvation in the O domains.

Introduction

Block polymers afford exciting opportunities to design nanostructured materials with hybrid functionalities for established and emerging technologies, including separation membranes,[1-3] organic solar cells,[4-6] and nanolithography templates.[7-9] The microstructured morphologies of narrow dispersity A/B di- and multi- block polymers depend on the volume composition ($f_A = 1 - f_B$) and the segregation strength χN, where χ is the effective segmental interaction parameter that quantifies the unfavorable A/B monomer contact energy and N is the degree of polymerization.[10, 11] Microphase separated A/B block polymers typically form lamellar (LAM), hexagonally-packed cylinders (HEX), spherical micelle packings (SPH), and bicontinuous network phases such as the double gyroid (GYR).[12, 13] For model narrow dispersity materials ($Đ = M_w/M_n \leq 1.2$), the consistency between experimental results[14, 15] and various mean-field theory calculations[16-18] powerfully enables flexible design of self-assembling A/B block polymers with high degrees of morphology control.

Over the last two decades, various reports have assessed the impacts of continuous segmental dispersity in both A/B di- and tri-block polymers on their phase behaviors as compared to their narrow dispersity analogues.[19] These studies were spurred by the development of polymer synthesis methodologies for producing functional block polymers with variable degrees of molar mass dispersity control.[20-26] Contrary to the notion that block polymers with broad segmental dispersities exhibit molecular-level "disorder" that forbids their thermodynamically-driven self-organization,[27] these materials experimentally assemble into microphase separated morphologies with varying degrees of long-range translational order.[24, 27-35] In AB diblocks comprising narrow dispersity A segments and broad dispersity B segments, Lynd and Hillmyer documented modest shifts in the observed phase windows and changes in the composition-dependent critical $(\chi N)_{ODT}$

for microphase separation at the order-disorder transition (ODT).[19, 29-31, 36] The groups of Leibler[27] and Mahanthappa[33, 37-40] further studied the impacts of broad A or broad B segment dispersity on the thermodynamics of ABA triblock polymer self-assembly, respectively.

Morphology diagrams for poly(styrene-*block*-1,4-butadiene-*block*-styrene) (SBS)[33, 40] and poly(lactide-*block*-1,4-butadiene-*block*-lactide) (LBL)[37, 38] triblocks with broad dispersity center segments ($Đ \sim 1.7–2.0$) exhibit both commonalties and differences in their phase behaviors. Widin *et al*. demonstrated that broad B segment dispersity in SBS triblocks lowers the critical segregation strength required for microphase separation to $(\chi N)_{ODT} \geq 4.5$ when $f_A \sim 0.5$, dilates the LAM microdomain spacing (d) by as much as two times, and shifts the LAM phase composition window to $0.55 \lesssim f_B \lesssim 0.75$.[33] In other words, the broad dispersity center segment apparently occupies a smaller than expected volume, favors interfacial curvature towards it, and stabilizes the ordered melt.[19] While the LAM composition window is similarly shifted in high χ/low N LBL triblocks, the LAM d-spacing and minimum $(\chi N)_{ODT}$ for microphase separation exhibit different trends. Schmitt and Mahanthappa showed that disperse B segments drive only 5–32% domain dilation in LBL triblocks, with a large increase in the critical segregation strength to $(\chi N)_{ODT} \geq 27$.[38] The d-spacing differences were ascribed to segregation strength differences, while the increased $(\chi N)_{ODT}$ was rationalized in terms of dispersity-amplified monomer concentration fluctuations at low N. These studies together suggest enticing opportunities to manipulate polymer morphology and thermodynamics by segmental dispersity control.[41, 42]

Toward solvent-free, solid-state electrolytes for advanced lithium-ion batteries, Balsara and co-workers have extensively studied the phase behaviors of poly(styrene-*block*-ethylene oxide) (SO) diblock polymers doped with lithium salts.[43-45] In these SO diblocks, lithium bis(trifluoromethylsulfonyl)imide (LiTFSI) selectively partitions into the O domains and drives

an overall increase in χ between the S and O/salt domains. Varying the amount of added LiTFSI in SO diblocks tunes χ over a wide range, leading to microphase separation in low N diblocks with increasing salt (*i.e.*, increasing χN).[43, 46, 47] These studies establish that variable salt doping provides a facile means for tuning segmental interaction strength in a given block polymer samples.[44] Thus, salt doping of broad dispersity block polymers offers a means for investigating apparent discrepancies in the phase behaviors of broad dispersity triblocks over a range segmental interaction strengths.

Herein, we report the syntheses and morphological studies of LiTFSI-doped poly(styrene-*block*-oligo(ethylene oxide) carbonate-*block*-styrene) triblock polymers with broad dispersity center O segments (bSOS) with $Đ_O = M_w/M_n \approx 1.45$ and narrow dispersity S segments ($Đ_S \leq 1.18$). Using a tandem polycondensation and atom transfer radical polymerization (ATRP) sequence, we synthesized 17 bSOS samples with $0.33 \leq f_O \leq 0.69$. Upon doping bSOS triblocks with varying amounts of LiTFSI, we mapped their morphology diagrams by temperature-dependent small-angle X-ray scattering (SAXS) as a function of Li-salt concentration. We compare these results to those from salt-doping 13 narrow dispersity SOS (nSOS) triblock control samples. These comparative studies reveal that the LAM phase window shifts to asymmetric volume compositions independent of salt-doping level, whereas the extent of LAM microdomain dilation in the bSOS samples decreases with increasing salt. Our studies further reveal that increased LiTFSI-doping of bSOS triblocks drives bSOS triblock microphase separation at lower N values with only a modest increase in $(\chi N)_{ODT}$. We rationalize these findings in terms of the competing effects of O segment dispersity that amplifies monomer concentration fluctuations and ordered state stabilization by preferential ion solvation in the O domains.

Experimental Methods

Materials. All reagents were purchased from Sigma-Aldrich Chemical Co. (Milwaukee, WI) and used as received unless otherwise noted. *N,N,N',N'',N''*-pentamethyldiethylenetriamine (PMDETA), Et_3N, and 2-bromoisobutyryl bromide were stirred over CaH_2 overnight, distilled under vacuum, and stored under nitrogen. Narrow dispersity poly(ethylene oxide) (PEO) with M_n = 1.4, 3.3, 4.6, 10, 20, 31 kg/mol and respective dispersities $Đ = M_w/ M_n$ = 1.12, 1.01, 1.02 1.03, 1.01, and 1.02 were freeze-dried from C_6H_6 and stored in a glovebox under inert atmosphere. Styrene was stirred over Brockman Type I basic alumina for 1 h at 25 °C and gravity filtered to remove inhibitors immediately prior to polymerization. CuBr was purified by a literature procedure.[48] Anhydrous and anaerobic tetrahydrofuran (THF) and CH_2Cl_2 were obtained by sparging analytical grade solvent with dry N_2(g) for 30 min, followed by cycling through a column of activated molecular sieves for 12 h in a Vacuum Atmospheres Co. (Hawthorne, CA) solvent purification system.

^{1}H Nuclear Magnetic Resonance (NMR) Spectroscopy. ^{1}H NMR spectra were acquired on a Bruker Avance III HD 400 MHz spectrometer in $CDCl_3$ and referenced to the residual protiated solvent resonance (δ 7.26 ppm). Polymer ^{1}H NMR spectra were acquired with a pulse repetition delay of 10-15 s to ensure quantitative peak integration accuracy for composition analyses.

Size-Exclusion Chromatography (SEC). SEC analyses for polyether and SOS block polymers relied on an Agilent 1200 Series GPC equipped with two Viscotek I-series columns (MBMMW-3078), a Wyatt Optilab T-rEX differential refractometer, and a Wyatt DAWN HELEOS II multi-angle laser light scattering detector operating at 50 °C in *N,N*-dimethylformamide (DMF) containing 0.05 M LiBr with a flow rate of 1.0 mL/min. For each narrow dispersity sample, the refractive index increment (*dn/dc*) was calculated assuming 100%

mass recovery upon sample elution. Polystyrene SEC analyses employed a Viscotek GPCMax System equipped with two Polymer Labs Resipore columns (250 mm x 4.6 mm) and a differential refractometer, running in THF at 40 °C with a flow rate of 0.8 mL/min. A polystyrene calibration curve was constructed with 10 narrow molar mass dispersity standards with M_n = 580-377,400 g/mol from Polymer Laboratories (Amherst, MA).

Representative Synthesis of Broad Dispersity α,ω-Di(bromoisobutyryl)-Poly(ethylene oxide) Carbonate (bPEOC-Br$_2$). Freeze-dried PEO (15.00 g, M_n = 1.4 kg/mol and $Đ$ = 1.12, 10.7 mmol) and NaH (60 *wt*% dispersion in mineral oil, 0.0436 g, 10.9 mmol) were combined in a 100 mL Schlenk tube in a glovebox. Outside of the glovebox on a vacuum line, diallyl carbonate (4.5 mL, 31.4 mmol) was added to the flask by syringe and a water-cooled distillation head with receiving flask was attached under a N_2(*g*) flush. The reaction tube was heated to 120 °C for 2 h under ambient pressure, after which the pressure was carefully reduced to 0.08 Torr and the reaction temperature was increased to 180 °C. The receiving flask was then chilled using a dry ice/2-propanol bath to condense the C_3H_5OH reaction byproduct and unreacted diallyl carbonate. The condensation reaction was continued for 20 min under these conditions. The resulting polymer was dissolved in CH_2Cl_2 (50 mL), precipitated into Et_2O (500 mL) twice, and dried under vacuum. $M_{n,\,SEC}$ = 13.5 kg/mol, $Đ$ = 1.56 and $M_{n,\,NMR}$ = 14.0 kg/mol.

The allyloxycarbonyl end groups of the resulting α,ω-diallylpoly(ethylene oxide) carbonate (5.00 g, 14.0 kg/mol, 0.36 mmol) were removed by treatment with $Pd(PPh_3)_4$ (0.0430 g, 0.037 mmol), PPh_3 (0.0385 g, 0.147 mmol) and 95 wt% formic acid (260 μL, 6.5 mmol) in anaerobic THF (150 mL) at 22 °C for 4 h.[49] Following solvent removal by rotary evaporation, the resulting α,ω-dihydroxy-poly(ethylene oxide) carbonate was redissolved in CH_2Cl_2 (50 mL), precipitated in Et_2O (500 mL) twice, and freeze-dried from minimal C_6H_6 to remove residual water.

The resulting α,ω-di(hydroxy)-poly(oligo(ethylene oxide) carbonate) (bPEOC) was dissolved in anhydrous CH_2Cl_2 (80 mL) and reacted with an excess of α-bromoisobutyryl bromide (270 μL, 2.2 mmol per –OH end group) and Et_3N (350 μL, 2.5 mmol per –OH end group). After solvent removal by rotary evaporation, the reaction mixture was redissolved in C_6H_6, filtered through a plug of Brockman Type I basic alumina, and precipitated into cold hexanes twice (500 mL). The resulting solids were freeze-dried from C_6H_6 to yield **bPEOC-Br$_2$**. $M_{n,\,SEC}$ = 12.8 kg/mol, $Đ$ = 1.48 and $M_{n,\,NMR}$ = 12.5 kg/mol.

Narrow dispersity α,ω-di(bromoisobutyryl)-poly(ethylene oxide) telechelics (**nPEO-Br$_2$**) were prepared from commercial, narrow dispersity PEO as previously reported.[50]

Representative Synthesis of bSOS Block Polymers. In an oven-dried 100 mL Schlenk flask, a mixture of styrene (30 mL, 262 mmol) and PMDETA (140 μL, 0.67 mmol) was subjected to three freeze-thaw degassing cycles. During the third freezing step, CuBr (0.096 g, 0.67 mmol) was quickly added to the frozen mixture under a flush of $N_2(g)$, after which the final evacuation and thaw cycle were completed. This mixture was stirred at 45 °C for 1 h under $N_2(g)$ to form the Cu-catalyst complex. 4.3 mL of this solution was added by syringe to a 25 mL Schlenk tube charged with **bPEOC-Br$_2$** (0.296 g, 0.0237 mmol) under $N_2(g)$ at 22 °C. The Schlenk tube was then heated to 90 °C in an oil bath. After 120 min, the reaction was stopped by cooling the Schlenk tube under cold running water. The reaction product was precipitated into rapidly stirred CH_3OH (20 mL) and stirred for 1 h. Residual solvent was removed from the resulting solids by rotary evaporation, after which they were dissolved in CH_2Cl_2 (5 mL), eluted through a short plug of basic $Al_2O_3(s)$ to remove Cu-catalyst residues, and precipitated into hexanes (30 mL). The isolated bSOS was freeze-dried from C_6H_6 and stored in a glovebox.

Narrow dispersity nSOS triblock polymers were similarly synthesized from **nPEO-Br$_2$**.

Representative SOS Block Polymer Degradation. bSOS_23.9_0.51 (50 mg) was dissolved in THF (0.5 mL) and treated with 2.5 M KOH in 50% *v*/*v* THF/ CH_3OH (2 mL). After reaction at 40 ºC for 12 h, the solution was precipitated into CH_3OH (10 mL) to isolate the S homopolymer. The solid polymer was freeze-dried from C_6H_6. $M_{n,SEC}$ = 5.4 kg/mol, $Đ$ = 1.11 (*versus* PS standards), and $M_{n,\,NMR}$ = 5.6 kg/mol.

Sample preparation. Block polymer samples (~30 mg) were dissolved in CH_2Cl_2 (0.5 mL), and measured amounts of LiTFSI in a 10% *v/v* solution THF/CH_2Cl_2 were added to achieve the desired r = [LiTFSI]/[EO units] based on M_n for each sample. Each solution was homogenized by sonication for 5 min and solvent cast into hermetic aluminum DSC pan bottoms (TA Instruments, Newcastle, DE) at 60 ºC. Samples were then heated to 140 °C under vacuum for 12 h to effect residual solvent and moisture removal, after which the DSC pans were hermetically sealed with the corresponding lids in a glovebox with [H_2O] ≤ 1 ppm.

Small Angle X-Ray Scattering (SAXS). Synchrotron SAXS measurements were conducted at the 12-ID-B beamline of the Advanced Photon Source (Argonne, IL). Using an incident beam energy of either 13.3 keV or 14.0 keV and a 3.605 m sample–to–detector distance, 2D–SAXS patterns were recorded on a Pilatus 2M area detector (25.4 cm × 28.9 cm active area with 1475 × 1679 pixel resolution) using exposure times of ~1 s. Block polymer samples were thermally equilibrated at each desired temperature in a multi-array sample stage for at least 10 min prior to X-ray analysis. All SAXS patterns were calibrated using a silver behenate standard (d = 58.38 Å), and reduced one-dimensional intensity $I(q)$ versus scattering wavevector q profiles were obtained using data reduction tools available at the beamline.

Results & Analysis

Synthesis and Molecular Characterization of bSOS. Unimodal bSOS triblock polymers with broad dispersity O segments were synthesized by a tandem polycondensation/atom transfer radical polymerization sequence (Scheme 1a and Figure 1a). By analogy to a reported polycarbonate synthesis,[51] condensation polymerization of an oligo(ethylene oxide) (M_n = 1.4 kg/mol) with diallyl carbonate catalyzed by NaH produced broad dispersity α,ω-diallylpoly(oligo(ethylene oxide) carbonate) samples with reaction time-dependent M_n values. The allyloxycarbonyl polymer end groups were removed by Pd(0)-catalyzed hydrogenolysis with HCOOH to furnish α,ω-dihydroxy-poly(oligo(ethylene oxide) carbonate) (bPEOC).[49] Esterification of bPEOC with α-bromoisobutyryl bromide yielded **bPEOC–Br$_2$** with M_n = 5.7–14.8 kg/mol and $Đ$ = 1.43–1.48. Number-average molecular weights calculated from ^{1}H NMR end group analyses concur with those obtained from SEC (within 15%), indicating a high degree of telechelic chain end functionality.[20] **bPEOC–Br$_2$** telechelics served as macroinitiators for (PMDETA)CuBr–catalyzed ATRP of styrene at 90 ºC to yield unimodal yet broad dispersity bSOS (Figure 1a). Block polymer compositions and polystyrene end segment molar masses were determined by quantitative ^{1}H NMR analyses based on the O midblock M_n's. Alkaline degradation of the bSOS triblocks with KOH in THF/CH_3OH (50:50 *v/v*) at 40 °C further enabled isolation and direct SEC characterization of the S end block M_n and $Đ$ (see Figure 1a for SEC trace overlay). By this method, we found that the S segments exhibit $Đ \leq 1.18$ and that the molar masses deduced by ^{1}H NMR and SEC agree within ~10%. Taken together, these data suggest the absence of unreacted bPEOC or any broad dispersity SO diblock contaminants.

The molecular characteristics of the bSOS triblock polymers produced by the above method are summarized in Table 1. Volume fractions for neat bSOS were calculated using the

homopolymer melt densities ρ_{PS} = 1.032 g/cm^3 and ρ_{PEO} = 1.073 g/cm^3 at 90 ºC.[52] Note that our use of the latter homopolymer melt density for PEO neglects the presence of carbonate linkages in the **bPEOC** (≤ 5.5 wt% per chain). The segment density-normalized degree of polymerization (N) based on a reference volume V_{ref} = 0.100 nm^3 was calculated as:[44]

$$N = \left(\frac{M_{n,\,PEO}}{\rho_{PEO}} + 2\frac{M_{n,\,PS}}{\rho_{PS}}\right)\Big/ N_A V_{ref}$$

where N_A is Avogadro's number. Samples are identified as bSOS_*x*_*y*, where *x* is the total $M_{n,SOS}$ (kg/mol) for the triblock and *y* is the O midblock volume fraction. Narrow dispersity SOS triblock polymers (nSOS) were synthesized via analogous Cu-mediated ATRP from narrow dispersity **nPEO-Br$_2$** (Scheme 1b). SEC characterization (Figure 1b) established the narrow dispersities of all constituent segments in these nSOS samples, for which molecular characteristics are also provided in Table 1.

Scheme 1. Syntheses of (a) bSOS Triblock Polymers via Tandem Polycondensation and ATRP and (b) nSOS Triblocks by ATRP.

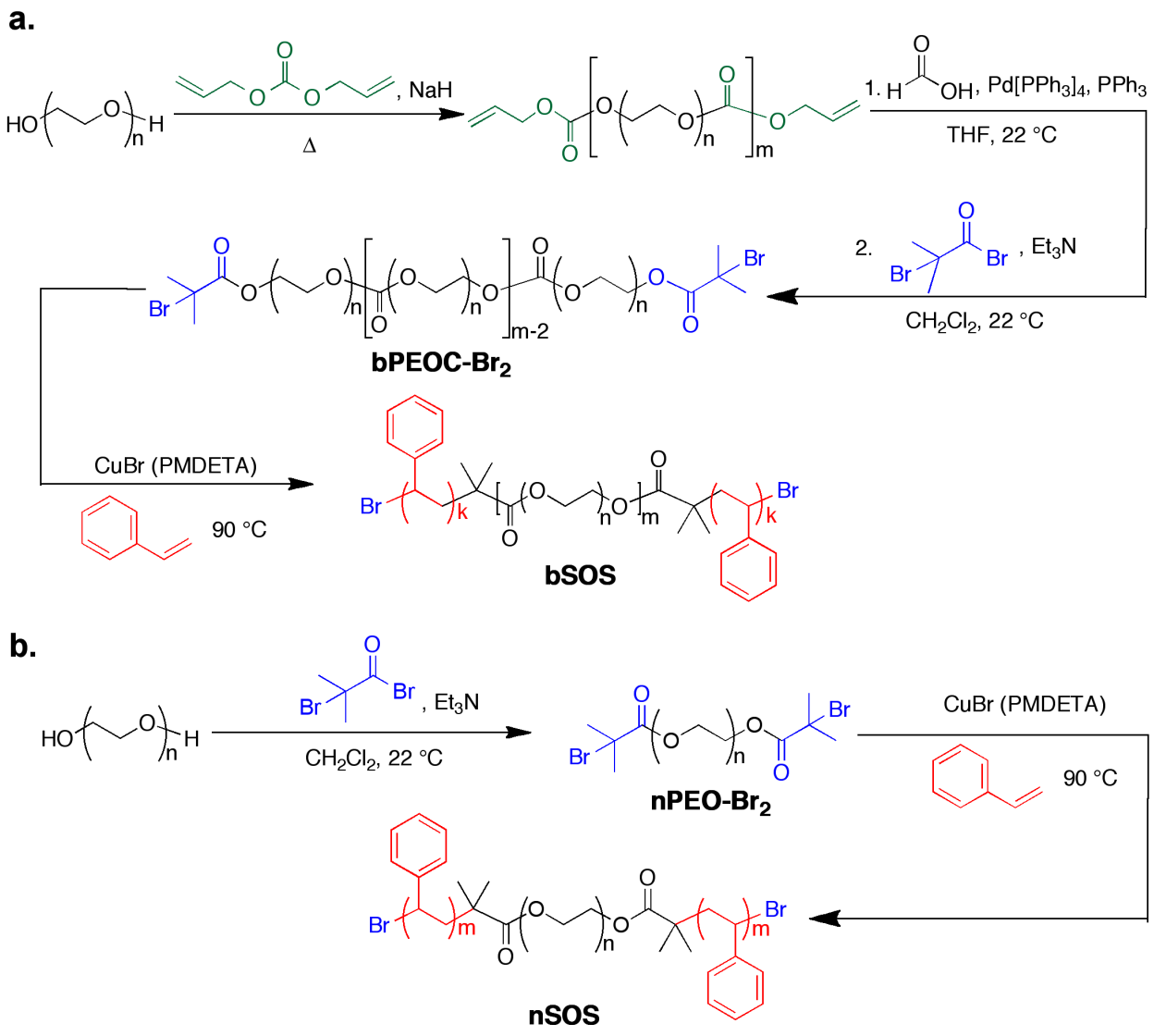

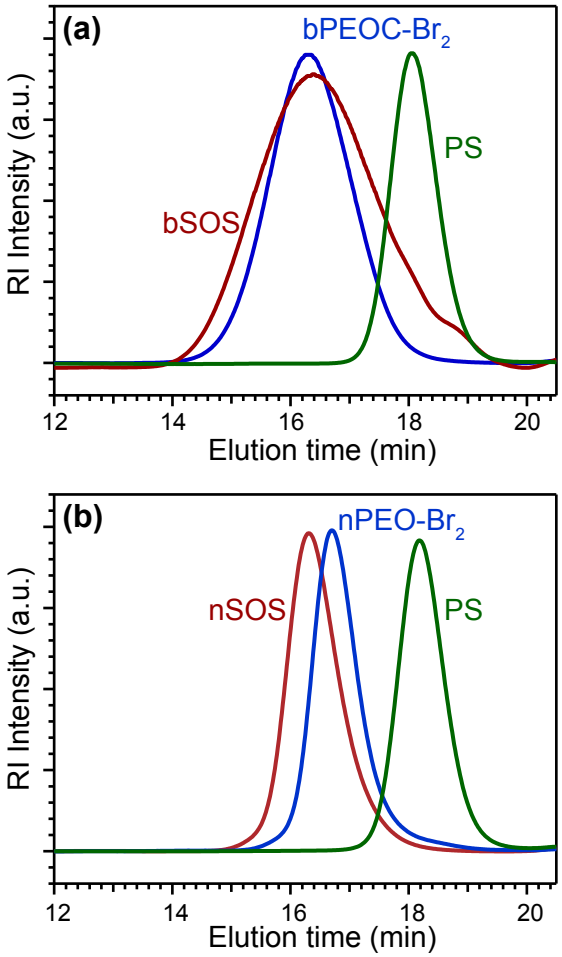

Figure 1. Representative SEC traces for (a) bSOS_23.9_0.51 and (b) nSOS_20.0_0.49 triblock polymers (*red*), the **bPEOC-Br$_2$** or **nPEO-Br$_2$** from which they derive (*blue*), and the PS homopolymer end segments derived from center block degradation (*green*).

Table 1. Molecular Characteristics of bSOS and nSOS Triblock Polymers.

		O midblock		S endblock		Block Polymer	
Sample	M_{n_SOS}[c]	$M_{n,NMR}$[a]	$Đ_{PEO}$[b]	$M_{n,NMR}$[c]	$Đ_{PS}$[d]	f_{EO}	N[e]
bSOS_43.8_0.33	43.8	14.8	1.45	14.5	1.12	0.33	696
bSOS_36.9_0.33	36.9	12.5	1.48	12.2	1.10	0.33	586
bSOS_32.9_0.37	32.9	12.5	1.48	10.2	1.12	0.37	522
bSOS_14.9_0.37	14.9	5.7	1.43	4.6	1.15	0.37	236
bSOS_38.0_0.38	38.0	14.8	1.45	11.6	1.13	0.38	603
bSOS_30.9_0.40	30.9	12.5	1.48	9.2	1.11	0.40	490
bSOS_11.7_0.48	11.7	5.7	1.43	3.0	1.18	0.48	185
bSOS_23.9_0.51	23.9	12.5	1.48	5.7	1.11	0.51	377
bSOS_23.2_0.52	23.2	12.4	1.48	5.4	1.13	0.52	366
bSOS_12.8_0.54	12.8	7.0	1.45	2.9	1.13	0.54	202
bSOS_12.2_0.56	12.2	7.0	1.45	2.6	1.14	0.56	192
bSOS_20.9_0.59	21.5	12.5	1.48	4.5	1.14	0.59	329
bSOS_24.8_0.59	24.8	14.8	1.45	5.0	1.15	0.59	390
bSOS_11.6_0.59	11.6	7.0	1.45	2.3	1.12	0.59	182
bSOS_19.6_0.62	19.6	12.4	1.48	3.6	1.13	0.62	308
bSOS_18.4_0.67	18.4	12.4	1.48	3.0	1.12	0.67	289
bSOS_21.2_0.69	21.2	14.8	1.45	3.2	1.15	0.69	332
nSOS_15.0_0.30	15.0	4.6	1.02	5.2	1.13	0.30	239
nSOS_12.8_0.35	12.8	4.6	1.02	4.1	1.11	0.35	203
nSOS_11.8_0.38	11.8	4.6	1.02	3.6	1.12	0.38	187
nSOS_11.2_0.40	11.2	4.6	1.02	3.3	1.13	0.40	177
nSOS_23.2_0.42	23.2	10.0	1.03	6.6	1.12	0.42	367
nSOS_45.2_0.43	45.2	20.0	1.01	12.6	1.14	0.43	715
nSOS_22.0_0.44	22.0	10.0	1.03	6.0	1.11	0.44	348
nSOS_7.1_0.46	7.1	3.3	1.03	1.9	1.11	0.46	112
nSOS_42.6_0.46	42.6	20.0	1.01	11.3	1.12	0.46	673
nSOS_20.0_0.49	20.0	10.0	1.03	5.0	1.12	0.49	316
nSOS_19.0_0.52	19.0	10.0	1.03	4.5	1.12	0.52	300
nSOS_8.4_0.54	8.4	4.6	1.02	1.9	1.16	0.54	132
nSOS_7.8_0.58	7.8	4.6	1.02	1.6	1.14	0.58	122

[a] Determined by quantitative end group analysis by ^{1}H NMR spectroscopy. [b] SEC in 0.05 M LiBr in DMF at 50 °C using *dn/dc* = 0.043 mL/g for **bPEOC-Br$_2$** and *dn/dc* = 0.042 mL/g for **nPEO-Br$_2$**. [c] Determined by quantitative ^{1}H NMR spectroscopy based on $M_{n,O}$. [d] Obtained by SEC in THF at 40 ºC versus narrow dispersity S homopolymer standards. [e] Calculated from neat polymer segment densities at 90 ºC using the reference volume V_{ref} = 0.100 nm^3.

Morphologies of Neat bSOS Triblocks. We first characterized the neat bSOS sample morphologies by SAXS between T = 22–150 °C. Salt-free bSOS samples with M_n < 25 kg/mol do not melt microphase separate, as only correlation-hole SAXS peaks were observed (Figure 2a).[53] When M_n > 30 kg/mol in the range f_O = 0.33–0.38, bSOS samples exhibit poorly ordered, microphase separated morphologies exemplified by the 1D-SAXS intensity profile for bSOS_38.0_0.38 at 22 °C (Figure 2a). This last sample appears to be microphase separated when T < 120 °C, since heating it to 120 °C leads to the disappearance of the broad, higher order reflections in a manner consistent with an order-disorder transition (see Supporting Information Figure S1). The broad, higher order peaks observed in these samples are located at (q/q*) = √1, √3, √4, √7, and √9 (q* = 0.020 Å^{-1}), consistent with poorly ordered, hexagonally-packed O cylinders in an S matrix (CYL_O). The observed peak breadths suggest poor translational order, analogous to that exhibited by broad dispersity block polymers with high M_n values.[33, 37, 54] The phase behaviors of the salt-free bSOS samples are compiled in the N versus f_O morphology diagram presented in Figure 2b.

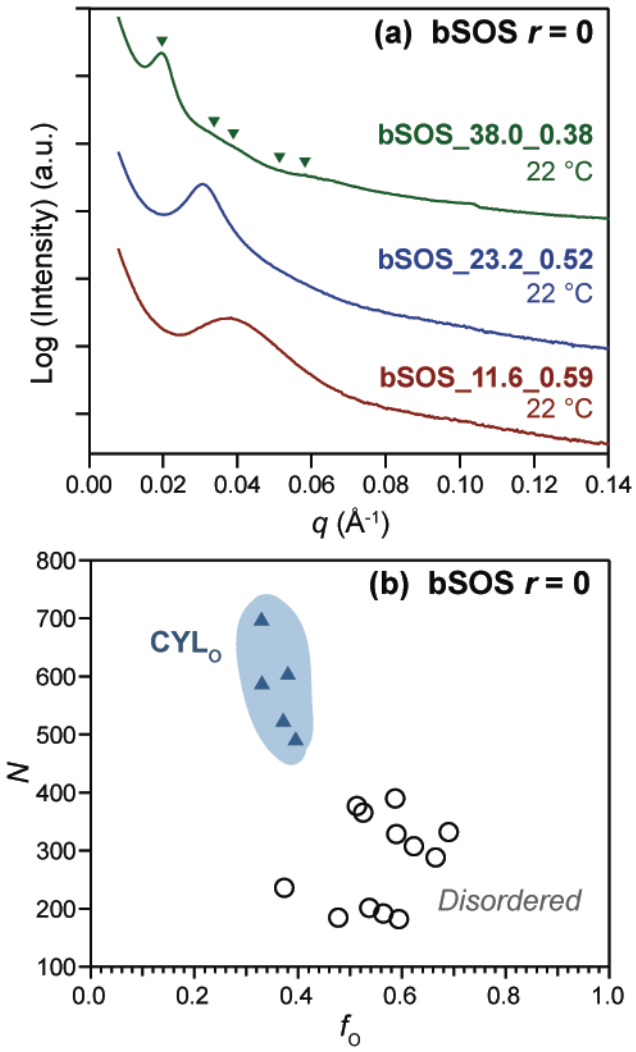

Figure 2. (a) 1D-SAXS profiles for neat bSOS triblock polymers, and (b) a bSOS morphology map for samples listed in Table 1 at T = 90 °C, where open circles (○) denote samples that are melt-disordered, solid triangles (▲) indicate ordered CYL_O samples.

Morphologies of LiTFSI-doped bSOS. The morphologies of bSOS triblocks doped with varying amounts of LiTFSI were also characterized by temperature–dependent synchrotron SAXS. Per the report of Teran and Balsara,[44] the volume fraction of the O/LiTFSI microphase was calculated as:

$$f_{\mathrm{O/salt}} = \frac{\frac{M_{\mathrm{n,\,PEO}}}{\rho_{\mathrm{PEO}}} + r\frac{M_{\mathrm{n,\,PEO}}}{M_{\mathrm{EO}}}\frac{M_{\mathrm{LiTFSI}}}{\rho_{\mathrm{LiTFSI}}}}{\frac{M_{\mathrm{n,\,PEO}}}{\rho_{\mathrm{PEO}}} + r\frac{M_{\mathrm{n,\,PEO}}}{M_{\mathrm{EO}}}\frac{M_{\mathrm{LiTFSI}}}{\rho_{\mathrm{LiTFSI}}} + 2\frac{M_{\mathrm{n,\,PS}}}{\rho_{\mathrm{PS}}}}$$

where $r = [Li^+]/[EO]$, M_{EO} and M_{LiTFSI} are the respective molar masses of ethylene oxide (44.05 g/mol) and LiTFSI (287.09 g/mol), and $\rho_{LiTFSI} = 2.023$ g/cm^3 is the effective LiTFSI density. This expression assumes complete segregation of LiTFSI into the O domains, as a consequence of polyether ligation to Li^+ and preferential anion solvation therein.[46, 55]

Minimal LiTFSI-doping at $r = 0.01$ significantly alters the melt self-assembly behavior of bSOS. In the range $f_{O/salt} = 0.33$–0.41 with $M_n \gtrsim 30$ kg/mol, SAXS analyses of the salt-doped bSOS (Figure 3a) reveal broad peaks possibly consistent with a hexagonally-packed cylinders (CYL) morphology. Increasing the volume fraction to $f_{O/salt} = 0.53$ yields a SAXS signature consistent with a double gyroid (GYR) morphology with peaks corresponding to the (211), (220), (321), (400), (420), (332), and (422) reflections with a lattice parameter $a = 53$ nm ($q_{(211)} = 0.029$ Å^{-1}). This observation constitutes the first report of a GYR morphology in any broad dispersity triblock polymer.[33, 37, 39] When $f_{O/salt} = 0.55$–0.70, high molar mass bSOS samples exhibit sharp primary SAXS peaks (q^*) with a higher order reflection at $2q^*$ (Figure 3a), which we identify as lamellae (LAM). Only the two samples with $M_n = 19.6$ and 21.2 kg/mol ($N = 308$ and 332) in this composition range at $r = 0.01$ exhibit accessible order-disorder transition temperatures $T_{ODT} = 139$ °C and 111 °C, respectively. Samples with $M_n < 19$ kg/mol ($N < 300$) display only the broad correlation-hole scattering of a disordered morphology. The phase sequence CYL →□GYR

→□LAM suggests that the GYR phase comprises LiTFSI-doped O cables in a S matrix (GYR_O), in spite of its occurrence at the majority salt volume fraction $f_{O/salt}$ = 0.53. These morphology data are summarized in Figure 3b.

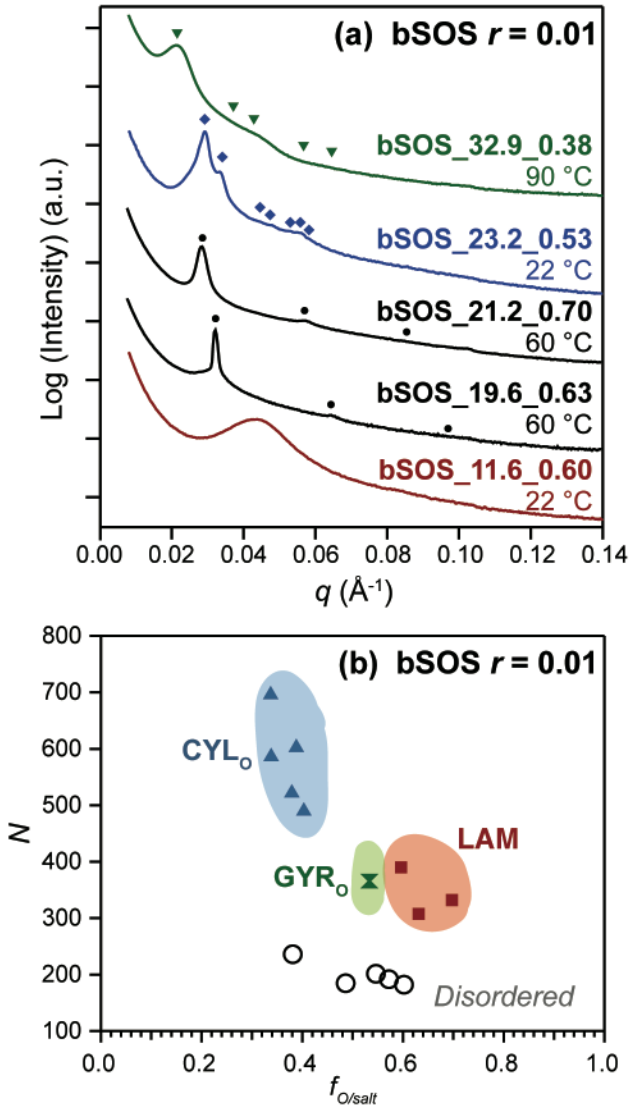

Figure 3. (a) Synchrotron SAXS intensity profiles for representative LiTFSI-doped bSOS triblock polymers with r = 0.01, in which symbols demarcate the calculated peak positions for CYL_O (*triangles*), GYR_O (*diamonds*), and LAM (*circles*). The peak at q = 0.104 Å^{-1} is an artifact associated with the detector mask. (b) A morphology diagram summarizing the results of SAXS

characterization of 14 salt-doped bSOS samples with $r = 0.01$ at $T = 90$ °C, where the colored regions are intended only to guide the eye and do not represent exact phase boundaries.

The somewhat surprising occurrence of GYR_O at $f_{O/salt} = 0.53$ led us to investigate the phase behaviors of nSOS control samples with comparable molecular weights. We synthesized nSOS per Scheme 1b, and nSOS molecular characterization data are given in Figure 1b and Table 1. SAXS data for selected samples at $r = 0.01$ provided in Figure 4a show that the narrow dispersity nSOS samples with $f_{O/salt} = 0.43$–0.45 and $M_n = 20.0$–23.2 kg/mol form GYR_O, while nSOS with a higher $M_n = 45.2$ kg/mol at $f_{O/salt} = 0.44$ instead forms LAM. Finally, we observe a composition-dependent order-order transition from $GYR_O \rightarrow$ LAM at $f_{O/salt} \approx 0.48$. Comparison of the N versus $f_{O/salt}$ morphology diagrams for bSOS (Figure 3b) and nSOS (Figure 4b) at $r = 0.01$ establishes that O segment dispersity in bSOS shifts the GYR and LAM phase windows by ~10 vol% toward higher $f_{O/salt}$. In other words, the salt-doped, broad dispersity O segment apparently occupies a smaller than expected volume.

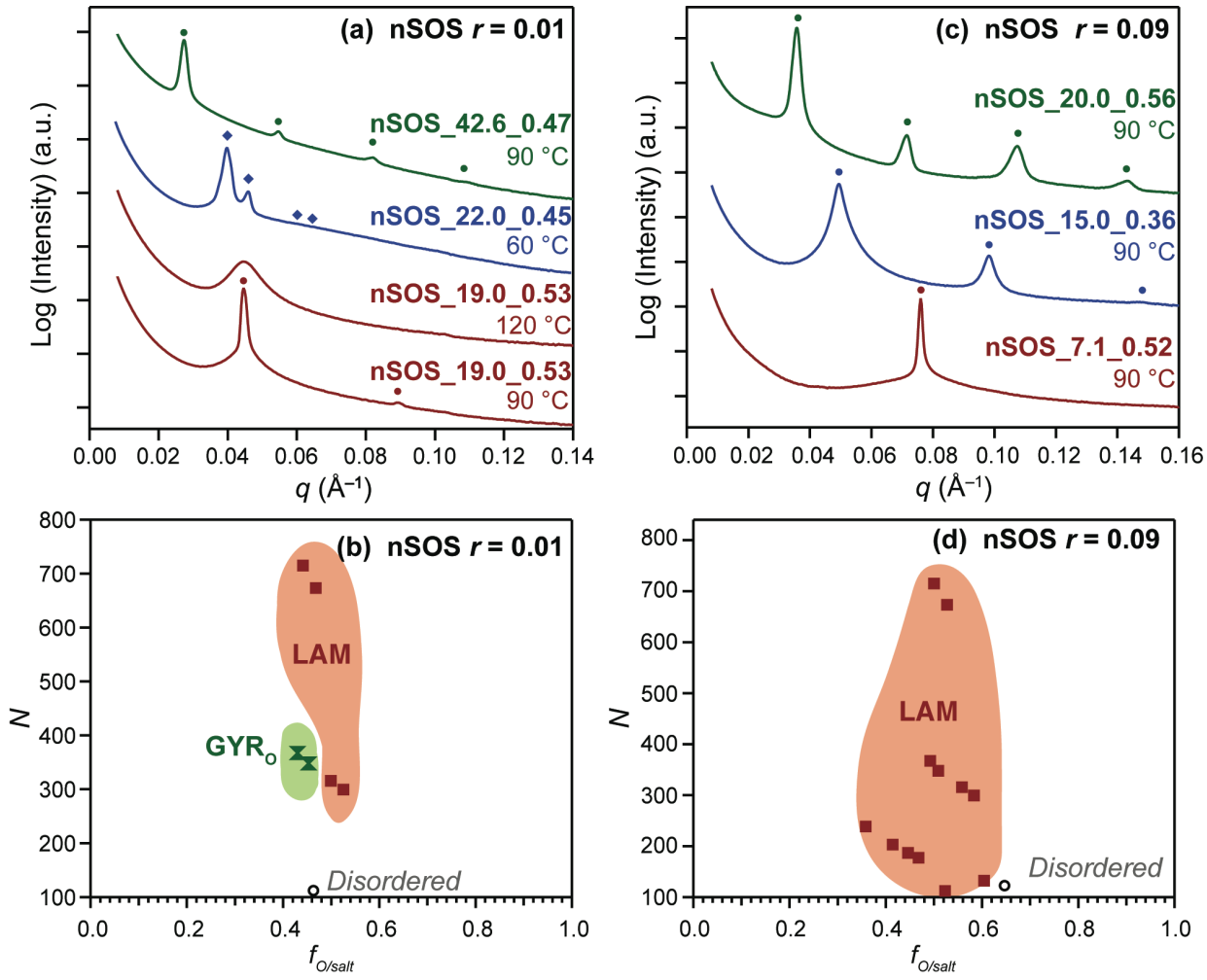

Figure 4. Synchrotron SAXS profiles for representative nSOS triblock polymers at (*a*) r = 0.01 and at (*c*) r = 0.09, wherein markers indicate the expected peak positions for GYR_O (*diamonds*) and LAM (*circles*). N versus $f_{O/salt}$ morphology diagrams for nSOS triblock polymers at T = 90 ºC (b) with r = 0.01 and (d) with r = 0.09 demonstrate increased salt-loading leads to the stabilization of LAM phases in the studied composition window.

Upon increasing the LiTFSI-doping level to r = 0.05, bSOS triblocks microphase separate with varying degrees of long-range translational order. At $f_{O/salt}$ = 0.41, we observe SAXS maxima at q/q^* = 1, √3, 2 and √7 (q^* = 0.036 $Å^{-1}$, Figure 5a), consistent with CYL_O with modest long-range

order. For samples with M_n > 30 kg/mol and $f_{O/salt}$ = 0.37–0.43 at r = 0.05, we observe poorly ordered yet segregated morphologies with broad SAXS peaks analogous to high M_n bSOS with r = 0.01 with similar $f_{O/salt}$ (Figure 3a). On that basis, we assign these samples as poorly ordered CYL_O. The sharper SAXS peaks observed in the low M_n CYL_O sample are consistent with greater chain mobility at low χN that enables structure refinement by thermal annealing. bSOS triblocks with asymmetric volume fractions $f_{O/salt}$ = 0.55–0.72 display SAXS intensity profiles with maxima at q/q^*= 1, 2, 3, and 4, corresponding to LAM. Note that the observed intensity and number of higher ordered SAXS peaks is greater for bSOS_19.6_0.66 with r = 0.05 (Figure 5a) than bSOS_19.6_0.63 with r = 0.01 (Figure 3a), even though both samples originate from the same parent bSOS polymer. Thus, increasing r drives bSOS self-assembly with better long-range order and sharper interfaces in a manner consistent with increased χN. bSOS_12.2_0.60 and bSOS_11.6_0.63, which are disordered at both r = 0 and 0.01, display accessible order-disorder transitions at T_{ODT} = 137 °C and 177 ºC, respectively. This observation is not unexpected as increasing r should increase melt segregation and thus T_{ODT}. Between the CYL_O and LAM phase windows at $f_{O/salt}$ = 0.52, we again observe a double gyroid morphology. bSOS_11.7_0.52 with r = 0.05 (Figure 5a) exhibits at least eight well-resolved peaks corresponding to GYR_O with a cubic unit cell parameter a = 39 nm ($q^*\sqrt{6}$ = 0.039 $Å^{-1}$). The occurrence of the (510) peak indicates significant long-range order, which contrasts the less well-organized structure noted for the higher M_n bSOS_23.2_0.53 at r = 0.01 (Figure 3a). The above morphology assignments are summarized in Figure 5b.

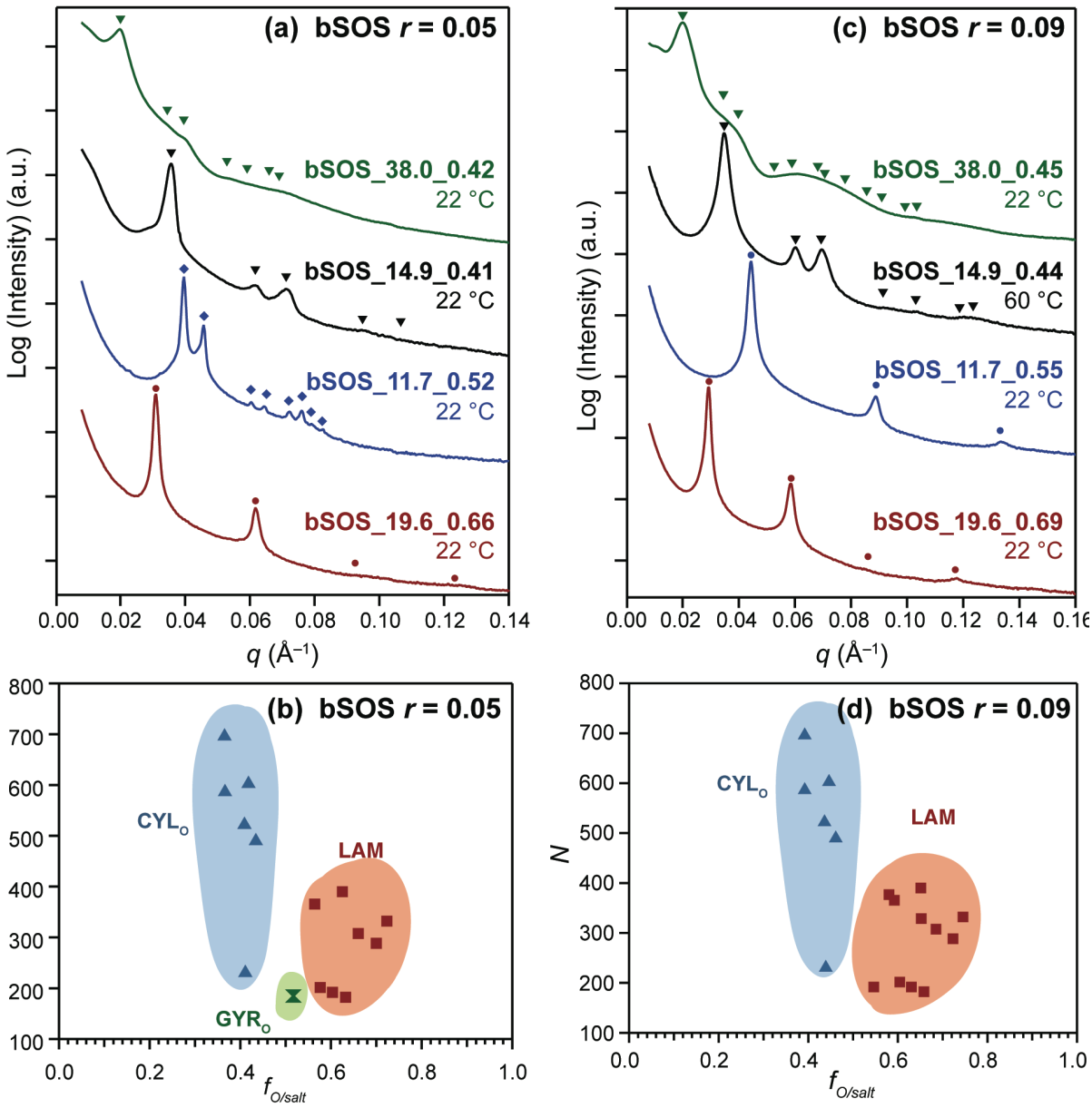

Figure 5. Azimuthally–integrated synchrotron SAXS patterns of representative bSOS triblock polymers with (a) r = 0.05 and (c) with r = 0.09, indicating the expected peak positions for CYL_O (*triangles*), GYR_O (*diamonds*), and LAM (*circles*) phases. N *versus* $f_{O/salt}$ morphology diagrams for (b) r = 0.05 and (d) r = 0.09 at 90 ºC.

The observed composition-dependent microphase windows for bSOS do not markedly change on further increasing the LiTFSI-doping level to $r = 0.09$, except that the GYR_O phase becomes inaccessible. We observe LAM in the asymmetric composition range $f_{O/salt} = 0.55–0.75$ and CYL_O when $f_{O/salt} = 0.39–0.46$ by SAXS (Figure 5c), as summarized in the morphology diagram in Figure 5d. bSOS_14.9_0.44 ($r = 0.09$) exhibits defined SAXS peaks at $(q/q^*)^2 = 1$, 3, 4, 7, and 9 corresponding to CYL_O, whereas the higher M_n bSOS_38.0_0.45 exhibits only the broad scattering of poorly-ordered CYL_O (Figure 5c) consistent with the above observations. At higher $f_{O/salt}$, bSOS_11.7_0.52 exhibits at least three Bragg peaks corresponding to LAM. While we cannot conclusively rule out the ability of bSOS to form GYR_O at $r = 0.09$, the GYR_O phase window width apparently narrows.

For control nSOS samples at $r = 0.09$, the data provided in Figures 4c and 4d establish that LAM form across the range $f_{O/salt} = 0.36–0.60$. Again, increasing $r = 0.01 \rightarrow 0.09$ also apparently extinguishes the GYR_O phase in these salt-doped polymers (*c.f.*, Figure 4b). Note that the GYR phase was previously observed to be unstable for $\chi N > 12$ in LiTFSI-doped narrow dispersity SO diblock polymers.[44] Thus, it appears that salt addition to S/O block polymers may generally restrict access to GYR phases regardless of center O segment dispersity.

Lamellar Domain Sizes in LiTFSI–Doped bSOS. Given that broad dispersity block polymers exhibit variable amounts of LAM domain dilation,[31-33, 38] we sought to quantitatively assess the extent of domain dilation in the salt-doped bSOS. Plots of lamellar *d*-spacings as a function of *N* at 90 °C for both nSOS and bSOS samples are given in Figure 6(a–c); see Supporting Information Tables S1–S3 for numerical values. From these plots, one readily observes that the extent of LAM domain dilation in bSOS for $r = 0.01$ is larger than that for $r = 0.05$ or 0.09. While the bSOS *d*-spacings are ~40% larger than those of corresponding nSOS

samples with comparable $f_{O/salt}$ and N (within 10%) at r = 0.01, we find a smaller extent of domain dilation of ~15–25% at the higher salt doping r = 0.05 and 0.09. Generally, the d-spacings of the nSOS triblocks monotonically increase with r, however the d increases with r in salt-doped in bSOS polymers are weaker as seen in Figure 6d: the addition of more LiTFSI to bSOS polymers triggers only small changes in d. Figure S2 shows data for other bSOS and nSOS with M_n = 19.0–45.2 kg/mol that exhibit comparable behaviors. Thus, for bSOS and nSOS samples of similar M_n, the d-spacing differences are larger at low salt concentrations and tend to decrease as r increases.

For each bSOS sample series at fixed r, we fit the LAM d-spacing data to the form $d \sim N^{\beta}$ to determine the scaling exponent β (fit shown in Figure 6). For r = 0.05, the scaling exponents for bSOS and nSOS are the same with $\beta_{b\mathrm{SOS}} = 0.64 \pm 0.08$ and $\beta_{n\mathrm{SOS}} = 0.64 \pm 0.04$, respectively. Increasing the salt-doping level to r = 0.09 results in a modest increase in the scaling exponent to $\beta_{b\mathrm{SOS}} = 0.69 \pm 0.07$ and $\beta_{n\mathrm{SOS}} = 0.73 \pm 0.02$. Since the last data positively deviate from $\beta = 2/3$ anticipated by strong segregation theory,[56, 57] we collected and analyzed literature data for the d-spacings of narrow dispersity SO diblock polymers at r = 0.085[58, 59] and found that $\beta_{n\mathrm{SO}} = 0.71 \pm 0.03$ (see Figure S3). These results collectively imply that block architecture and dispersity differences do not appreciably affect β for $r \geq 0.05$.

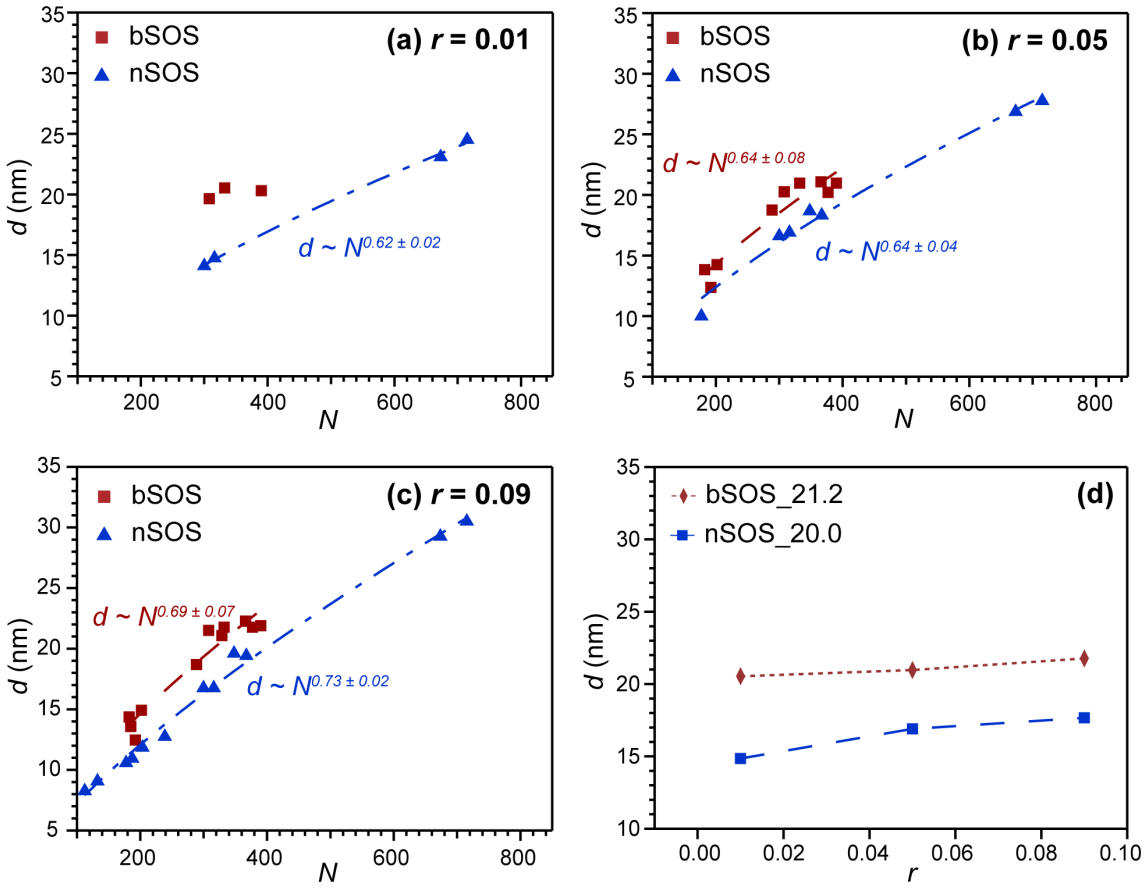

Figure 6. Lamellar *d*-spacing comparison for bSOS (*squares*), nSOS (*triangles*) at r = [LiTFSI]/[EO] = (a) 0.01, (b) 0.05, and (c) 0.09, for which the dashed line represents the power law fit used to obtain β, and (d) *d*-spacings for representative bSOS (*red*) and nSOS (*blue*) triblock polymers with increasing r.

Salt-Doping Dependence of Order and Disorder. SAXS offers a convenient means for determining the ODT temperature (T_{ODT}), at which the Bragg scattering associated with the ordered block polymer morphology evolves into correlation-hole scattering of a disordered melt. The ODT for bSOS_19.6_0.63 at r = 0.01 is relatively broad, as the principal reflection (q^*) gradually diminishes in intensity over a range of temperatures (Figure 7). We assign T_{ODT} as the temperature at which the sharp q^* peak completely vanishes. The transition breadth is not wholly

unexpected, as Gibbs' Phase Rule anticipates a window of two-phase coexistence between the ordered and disordered states (assuming a pseudo-two component mixture of bSOS and LiTFSI). Similarly, broad ODT's have been previously observed and rationalized by mean-field theories for salt-doped systems.[60-62] Table 2 lists bSOS and nSOS samples that exhibited accessible T_{ODT}'s at different r-values. While the bSOS_19.6_0.63 exhibits T_{ODT} = 139 °C, bSOS_21.2_0.70 with r = 0.01 exhibits a lower T_{ODT} = 111 °C suggesting its closer proximity to the microphase separation transition. At the higher salt concentration r = 0.05, samples with accessible T_{ODT}'s exhibit much lower M_n's than those with r = 0.01. bSOS_11.6_0.63 exhibits T_{ODT} = 177 °C, whereas T_{ODT} = 137 °C of bSOS_12.2_0.60 with the same salt loading r = 0.05. This last observation indicates a strong composition dependence of T_{ODT} in these broad dispersity triblocks, given that these two samples stem from the same *b*PEOC midblock.

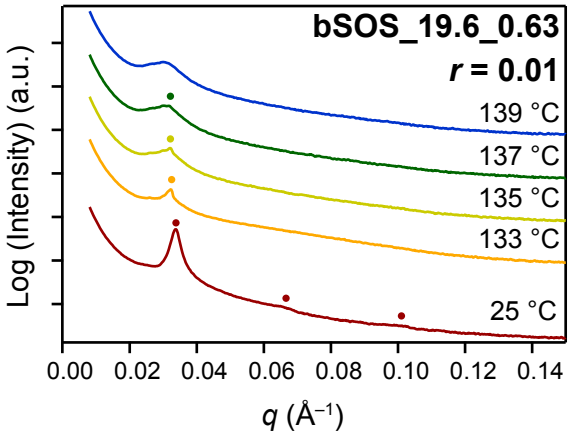

Figure 7. Temperature-dependent synchrotron SAXS profile for bSOS_19.6_0.63 showing the formation of LAM at 25 °C, with T_{ODT} = 139 °C at which the sharp principal (q^*) peak is absent, and only broad correlation-hole scattering of the disorder state is observed.

Table 2. T_{ODT} and calculated $(\chi N)_{ODT}$ for bSOS and nSOS triblocks at r = 0.01 and 0.05.

r	0.01		0.05	
Sample	bSOS_19.6_0.63	bSOS_21.2_0.70	bSOS_12.2_0.60	bSOS_11.6_0.63
T_{ODT} (°C)	139	111	137	177
$(\chi_{eff}N_{di})_{ODT}$	10.3	10.8	11.1	10.8
Sample	nSOS_19.0_0.53	nSOS_20.0_0.50	nSOS_11.2_0.44	
T_{ODT} (°C)	141	148	189	
$(\chi_{eff}N_{di})_{ODT}$	10.2	10.2	10.7	

We used the f_O-independent effective segmental interaction parameter $\chi_{eff}(T)$ developed by Teran *et al.*[44] for LiTFSI-doped SO diblocks at a given r-value

$$\chi_{eff}(T)=\frac{10.2}{T}+\frac{1.85\times10^{3}}{T\cdot N_{di}}+\frac{1.01\times10^{-2}\cdot T}{N_{di}}\left[1\text{-}\exp\left(\frac{\text{-}22.4\cdot Tr}{N_{di}}\right)\right]$$

to calculate the segregation strengths $\chi_{eff}N_{di} = \chi_{eff}N/2$ □associated with each sample described here, in order to recast the phase information determined for bSOS and nSOS with r = 0.01 and 0.05 (Figures 3b, 4b, and 5b) into $\chi_{eff}N_{di}$ *versus* $f_{O,salt}$ morphology diagrams. This complex χ_{eff} expression was derived by fitting the absolute disordered state SAXS intensity from LiTFSI-doped SO diblock polymers to the random phase approximation,[44] wherein N_{di} is the segment density-normalized degree of polymerization of the neat diblock with respect to the reference volume V_{ref} = 0.1 nm^3. In spite of disagreements in the literature regarding the best r-dependent functional form that describes $\chi_{eff}(T)$ for LiTFSI-doped S/O block polymers, use of this expression for salt-doped SO diblock polymers with reported T_{ODT} values gives $(\chi_{eff}N)_{ODT}$ = 9.7–10.8 for $0 \leq r \leq 0.10$, consistent with the mean-field theory prediction $(\chi_{eff}N)_{ODT}$ = 10.495. The

use of this conceptual framework enables more direct comparisons of the morphology diagrams of salty bSOS samples described here with those reported for other disperse, non-ionic A/B block polymers with different chemistries based on effective segmental interaction parameters (χ_{eff}) also derived from mean-field theories. Additionally, this formalism may help to guide the synthesis of bSOS samples with specific attributes for future studies.

Morphology diagrams for bSOS and nSOS constructed using this particular formalism for r = 0.01 and 0.05 are presented in Figure 8, and the $(\chi_{eff}N_{di})_{ODT}$ values for samples showing accessible order-disorder transitions are given in Table 2. From nSOS_20.0_0.50 with r = 0.01, we calculate a critical $(\chi_{eff}N_{di})_{ODT}$ = 10.2 for microphase separation. Although mean-field theory for ABA-triblock polymers anticipates that $(\chi N_{di})_{ODT} \geq 8.95$ for microphase separation,[63] the $\chi_{eff}(T)$ of Teran *et al*.[44] likely does not account for segment connectivity (architecture) effects nor the impact of monomer concentration fluctuations.[64] We observe a similar deviation from the expected mean-field result for nSOS_11.2_0.44 with r = 0.05, for which $(\chi_{eff}N_{di})_{ODT}$ = 10.7. Inspection of the morphology maps for bSOS in Figure 8 (and Table 2) shows that for the bSOS triblocks, $(\chi_{eff}N_{di})_{ODT} \geq 10.3$ for r = 0.01 and $(\chi_{eff}N_{di})_{ODT} \geq 10.8$ for r = 0.05. Thus, increased salt-doping of the bSOS samples only slightly increases $(\chi N)_{ODT}$ for microphase separation over that for the control nSOS samples.

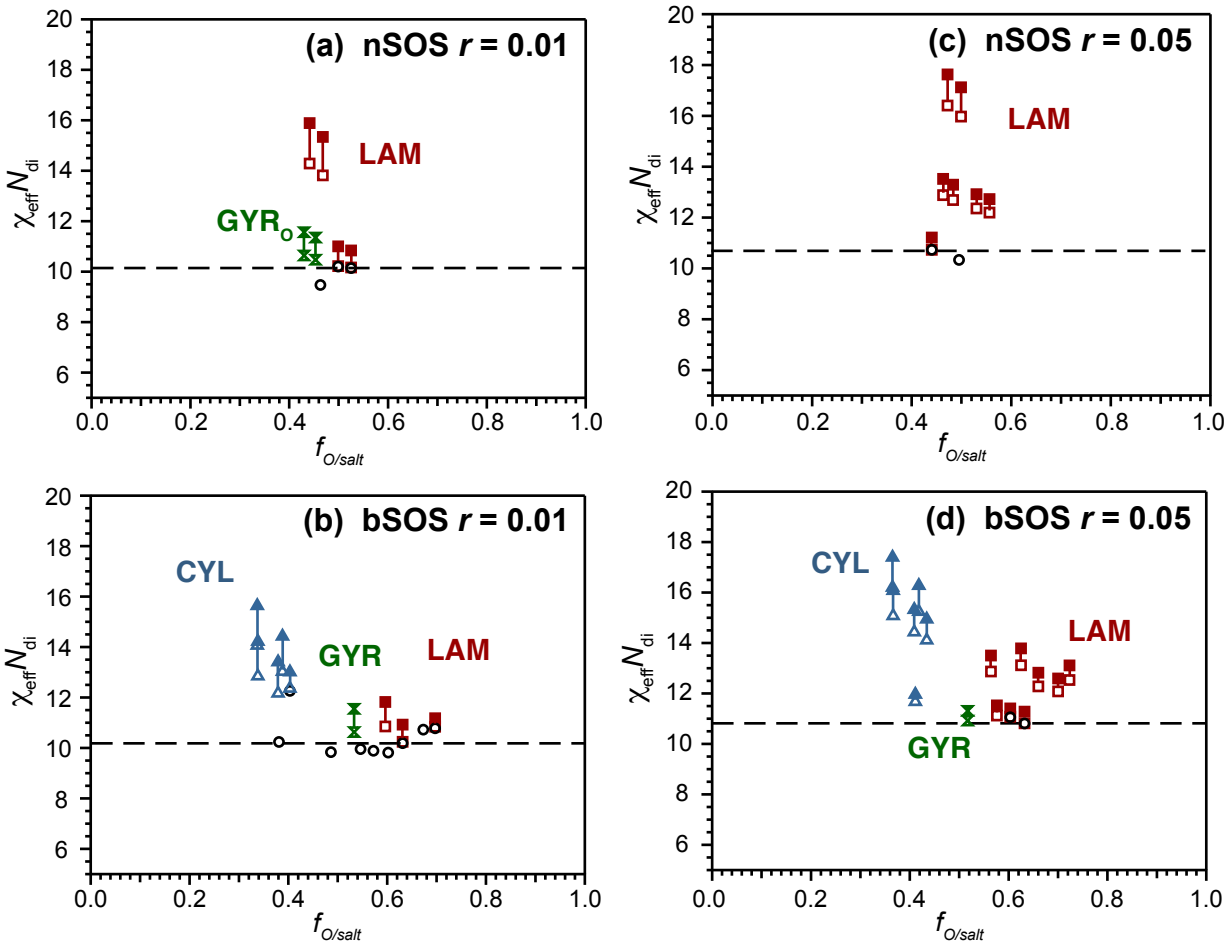

Figure 8. ($\chi_{eff}N$) versus $f_{EO/salt}$ morphology diagrams at $r = 0.01$ for (a) nSOS and (b) bSOS, and at $r = 0.05$ for (c) nSOS and (d) bSOS at a reference temperature $T_{ref} = 90$ °C. The vertical lines indicate the range of temperatures over which the morphologies were determined by SAXS, and those lines capped with black open circles indicate samples that disordered on heating. The dashed line is drawn to indicate the minimum observed $(\chi_{eff}N_{di})_{ODT}$ at a given salt-doping level r.

Discussion

A few reports have documented segmental dispersity-induced dilation of the lamellar *d*-spacings of ABA triblocks with broad dispersity B midblocks, which stems from the broad chain length distribution and is likely sensitive to its exact width and shape.[24, 36] Generally, *d*-spacing dilation has been ascribed to two synergistic effects: (1) the presence of much longer than average B segments that fill space, and (2) interfacial desorption of ABA chains with short B segments that effectively act as "A–A homopolymers" that swell the A domains.[33] Lynd *et al*. described a method for calculating the critical B segment M_n below which chain desorption occurs, by equating the enthalpy cost for dissolving a short B segment in the A domain and the entropy gain from releasing the stretched chains from the domain interfaces.[36] They showed that the critical desorption chain length scales as $(\chi N)^{-2/3}$, thus predicting reduced *d*-spacing dilation in strongly segregated polymers due to suppressed chain pull out.

By virtue of the ability to tune χ_{eff} at constant N in a given bSOS by varying the salt-doping level r, our data provide an opportunity to analyze how *d*-spacing dilation changes with melt segregation strength. The data shown in Figure 6 indicate that the extent of domain dilation is greatest at $r = 0.01$ and that less domain dilation occurs when $r = 0.05$ and 0.09. These results may be rationalized by first considering how lamellar *d*-spacing depends on r for nSOS. In salt-doped nSOS, d increases with r since the O domain volume is augmented by the preferential solvation of LiTFSI and the concomitant increase in χ between the S and LiTFSI-doped O-domains leads to chain stretching. While these physical principles apply to bSOS and should drive *d*-spacing increases, the overall increase in χN raises the enthalpic penalty for interfacial chain desorption and decreases the extent of "A-A homopolymer" swelling (*vide supra*).

Apparently, these two effects cancel and result in the observed weak dependence of d on the doping level, r.

The LAM window shift to asymmetric volume fractions $f_{O/salt} \approx 0.55–0.75$ irrespective of bSOS salt doping level (r) is nearly identical to the dispersity-induced lamellar composition shifts previously reported in SBS[33] and LBL triblocks[38] with broad dispersity B segments. Given the low degree of "S–S homopolymer" swelling in the strongly segregated LiTFSI-doped bSOS, this LAM morphology window shift must arise from synergistic chain packings in the disperse O/salt microdomain that foster buckling towards it in a manner similar to that noted in LBL triblocks.[38] The details of this co-surfactant-like chain packing that fosters curvature toward the disperse domain have been explained elsewhere[33,65] and are not reiterated here.

In contrast to previous studies that found either large increases or decreases in the critical $(\chi_{eff}N_{di})_{ODT}$ for microphase separation of ABA-type triblocks with broad dispersity B segments,[33, 37] the critical $(\chi_{eff}N_{di})_{ODT}$ for salt-doped bSOS only marginally increases from the expected value of $(\chi_{eff}N_{di})_{ODT} = 8.95$ for narrow dispersity materials. In the case of SBS triblocks with broad dispersity B segments, the segregated melt is stabilized by synergistic interfacial chain packings of the medium and long chains in the distribution that decrease center segment chain stretching. This result concurs with self-consistent mean-field theory (SCFT) calculations by Matsen for such systems.[65] However, center B segment dispersity in high χ/low N LBL triblocks amplifies monomer concentration fluctuations that destabilize the ordered morphologies. The magnitude of this destabilization apparently overwhelms the synergistic chain packing stabilization, leading to a net increase in the critical $(\chi N)_{ODT}$.[37] Modified SCFT calculations by Pandav and Ganesan[66] and Monte Carlo simulations by Beardsley and Matsen[67] indicate that dispersity enhances

fluctuation effects, as experimentally demonstrated for nearly monodisperse diblock oligomers by Oschmann and co-workers.[68]

The modest changes in $(\chi N)_{ODT}$ for salt-doped bSOS likely arise from a combination of two opposing factors depicted in Figure 9. While O segment dispersity is expected to enhance monomer concentration fluctuations and drive up $(\chi N)_{ODT}$, preferential solvation of LiTFSI in the O domains increases segment incompatibility and drives microphase separation in a manner that counters the enhanced concentration fluctuations.[46, 69, 70] Additionally, lithium ions in the salt-doped O domains are coordinated by 2–7 O monomer units from one or several polymer chains, which may serve to dynamically crosslink these domains.[71-73] Ren *et al.*[74] have proposed a model in which they predict that preferential anion solvation and dynamic lithium salt crosslinks synergistically enhance microphase separation, and recent experiments by Xie and Lodge[75] suggest that similar effects drive blend phase separation in salty poly(ethylene-*alt*-propylene)/PEO. Consequently, the effect of salt solvation in the O domain dominates, yielding only small changes in the critical $(\chi_{eff}N_{di})_{ODT}$ upon LiTFSI salt doping of bSOS.

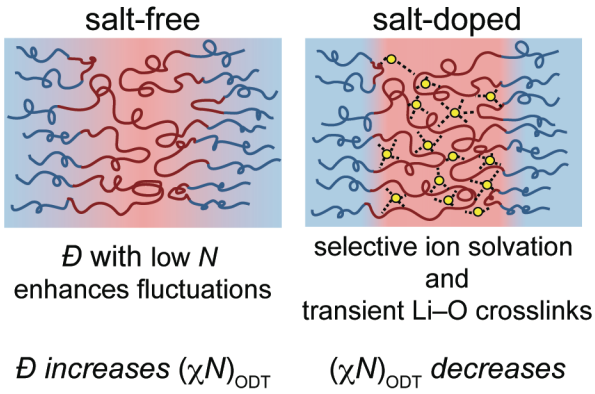

Figure 9. For high χ/low N salt-doped bSOS, (a) broad dispersity low N polymer chains enhance fluctuation effects thereby disfavoring microphase separation, while (b) solvation of LiTFSI in the O domains leads to increased segment incompatibility as well as dynamic crosslinking of the O segments, both of which stabilize the ordered morphology.

This notion is further supported by a detailed comparison of the phase behaviors of bSOS doped with LiTFSI at r = 0.01 and 0.05. From the data presented in Table 2, one finds that the $(\chi_{eff}N_{di})_{ODT}$ ~ 10.2 at r = 0.01 with overall M_n = 19.6–21.2 kg/mol. On the other hand, $(\chi_{eff}N_{di})_{ODT}$ ~ 11 for samples with r = 0.05 and M_n = 11.6–12.2 kg/mol. This modest difference in the critical segregation strength for microphase separation follows the expected trend that the fluctuation corrections for lower molecular weight systems are stronger and lead to slightly greater destabilization of the microphase separated morphology.

Conclusion

In this work, we described the synthesis and characterization of seventeen unimodal yet continuously disperse bSOS polymers by a sequential condensation polymerization and ATRP, to furnish broad dispersity O midblocks flanked by narrow dispersity S end blocks with $0.33 \leq f_O \leq 0.69$ and $11.7 \leq M_n \leq 43.8$ kg/mol. Temperature-dependent SAXS analyses were used to construct morphology maps of bSOS samples doped with varying amounts of LiTFSI at salt loading levels r = 0–0.09. Generally, the bSOS lamellar phase window shifts by ~10 vol% to higher $f_{O/salt}$ based on direct comparisons with 13 narrow dispersity nSOS analogs that were characterized at the same LiTFSI loadings. Additionally, midblock dispersity dilates the lamellar

microdomain *d*-spacing, although the extent of domain dilation depends on the specific *r*-value. The critical segregation strength for microphase separation is found to be $(\chi N/2)_{ODT} \geq 10.3$ for $r = 0.01$, whereas $(\chi N/2)_{ODT} \geq 10.8$ for $r = 0.05$. Thus, segmental dispersity in salt-doped polymers only incrementally increases the critical segregation strength from the mean-field theory prediction $(\chi N/2)_{ODT} = 8.95$. This last result contrasts previous work on ABA-type triblock polymers in which mid-segment dispersity results in larger changes in the location of the microphase separation transition. We attribute the present findings in the salty bSOS to a competition between dispersity-enhanced fluctuations in these high χ/low N materials near the ODT and preferential lithium salt solvation in the O domains that stabilizes the ordered melts.

Associated Content

Notes

The authors declare no competing financial interests.

Supporting Information

Temperature dependent 1D-SAXS patterns for bSOS_38.0_0.38; lamellar *d*-spacing and the power-law fitting for nSO diblock polymers at $r = 0.085$; lamellar *d*-spacings of salt-doped bSOS and nSOS at $r = 0.01$, 0.05 and 0.09, respectively.

Acknowledgments

This work was supported by National Science Foundation grants DMR–1307606, DMR–1631598, DMR–1708874. Synchrotron SAXS experimented were conducted at the 12-ID-B beamline of the Advanced Photon Source, a U.S. Department of Energy (DOE) Office of

Science User Facility operated by Argonne National Laboratory under contract no. DE-AC02-06CH11357. We thank Grayson L. Jackson and Tyler J. Mann for helpful discussions.

References

1. Olson, D. A.; Chen, L.; Hillmyer, M. A. Templating Nanoporous Polymers with Ordered Block Copolymers. *Chem. Mater.* **2008,** *20*, 869-890.

2. Abetz, V. Isoporous Block Copolymer Membranes. *Macromol. Rapid Commun.* **2015,** *36*, 10-22.

3. Werber, J. R.; Osuji, C. O.; Elimelech, M. Materials for Next-Generation Desalination and Water Purification Membranes. *Nature Rev. Mater.* **2016,** *1*, 16018.

4. Crossland, E. J. W.; Kamperman, M.; Nedelcu, M.; Ducati, C.; Wiesner, U.; Smilgies, D. M.; Toombes, G. E. S.; Hillmyer, M. A.; Ludwigs, S.; Steiner, U.; Snaith, H. J. A Bicontinuous Double Gyroid Hybrid Solar Cell. *Nano Lett.* **2009,** *9*, 2807-2812.

5. Orilall, M. C.; Wiesner, U. Block Copolymer Based Composition and Morphology Control in Nanostructured Hybrid Materials for Energy Conversion and Storage: Solar Cells, Batteries, and Fuel Cells. *Chem. Soc. Rev.* **2011,** *40*, 520-535.

6. Yoo, H. G.; Byun, M.; Jeong, C. K.; Lee, K. J. Performance Enhancement of Electronic and Energy Devices via Block Copolymer Self-Assembly. *Adv. Mater.* **2015,** *27*, 3982-3998.

7. Cheng, J. Y.; Ross, C. A.; Smith, H. I.; Thomas, E. L. Templated Self-Assembly of Block Copolymers: Top-Down Helps Bottom-Up. *Adv. Mater.* **2006,** *18*, 2505-2521.

8. Bang, J.; Jeong, U.; Ryu, D. Y.; Russell, T. P.; Hawker, C. J. Block Copolymer Nanolithography: Translation of Molecular Level Control to Nanoscale Patterns. *Adv. Mater.* **2009,** *21*, 4769-4792.

9. Bates, C. M.; Maher, M. J.; Janes, D. W.; Ellison, C. J.; Willson, C. G. Block Copolymer Lithography. *Macromolecules* **2014,** *47*, 2-12.

10. Bates, F. S.; Fredrickson, G. H. Block Copolymer Thermodynamics : Theory and Experiment. *Annu. Rev. Phys. Chem.* **1990,** *41*, 525-557.

11. Leibler, L. Theory of Microphase Separation in Block Copolymers. *Macromolecules* **1980,** *13*, 1602-1617.

12. Abetz, V.; Simon, P. F. W. Phase Behaviour and Morphologies of Block Copolymers. *Adv. Polym. Sci.* **2005,** *189*, 125-212.

13. Bates, F. S.; Hillmyer, M. A.; Lodge, T. P.; Bates, C. M.; Delaney, K. T.; Fredrickson, G. H. Multiblock Polymers: Panacea or Pandora's Box? *Science* **2012,** *336*, 434-440.

14. Khandpur, A. K.; Förster, S.; Bates, F. S.; Hamley, I. W.; Ryan, A. J.; Bras, W.; Almdal, K.; Mortensen, K. Polyisoprene-Polystyrene Diblock Copolymer Phase Diagram near the Order-Disorder Transition. *Macromolecules* **1995,** *28*, 8796-8806.

15. Mai, S. M.; Mingvanish, W.; Turner, S. C.; Chaibundit, C.; Fairclough, J. P. A.; Heatley, F.; Matsen, M. W.; Ryan, A. J.; Booth, C. Microphase-Separation Behavior of Triblock Copolymer Melts. Comparison with Diblock Copolymer Melts. *Macromolecules* **2000,** *33*, 5124-5130.

16. Cochran, E. W.; Garcia-Cervera, C. J.; Fredrickson, G. H. Stability of the Gyroid Phase in Diblock Copolymers at Strong Segregation. *Macromolecules* **2006,** *39*, 2449-2451.

17. Matsen, M. W. Effect of Architecture on the Phase Behavior of AB-Type Block Copolymer Melts. *Macromolecules* **2012,** *45*, 2161-2165.

18. Arora, A.; Qin, J.; Morse, D. C.; Delaney, K. T.; Fredrickson, G. H.; Bates, F. S.; Dorfman, K. D. Broadly Accessible Self-Consistent Field Theory for Block Polymer Materials Discovery. *Macromolecules* **2016,** *49*, 4675-4690.

19. Lynd, N. A.; Meuler, A. J.; Hillmyer, M. A. Polydispersity and Block Copolymer Self-Assembly. *Prog. Polym. Sci.* **2008,** *33*, 875-893.

20. Bielawski, C. W.; Morita, T.; Grubbs, R. H. Synthesis of ABA Triblock Copolymers via a Tandem Ring-Opening Metathesis Polymerization: Atom Transfer Radical Polymerization Approach. *Macromolecules* **2000,** *33*, 678-680.

21. Monteiro, M. J. Design Strategies for Controlling the Molecular Weight and Rate Using Reversible Addition–Fragmentation Chain Transfer Mediated Living Radical Polymerization. *J. Polym. Sci. Part A: Polym. Chem.* **2005,** *43*, 3189-3204.

22. Arriola, D. J.; Carnahan, E. M.; Hustad, P. D.; Kuhlman, R. L.; Wenzel, T. T. Catalytic Production of Olefin Block Copolymers via Chain Shuttling Polymerization. *Science* **2006,** *312*, 714-719.

23. Plichta, A.; Zhong, M.; Li, W.; Elsen, A. M.; Matyjaszewski, K. Tuning Dispersity in Diblock Copolymers Using ARGET ATRP. *Macromol. Chem. Phys.* **2012,** *213*, 2659-2668.

24. Gentekos, D. T.; Jia, J.; Tirado, E. S.; Barteau, K. P.; Smilgies, D. M.; Distasio, R. A.; Fors, B. P. Exploiting Molecular Weight Distribution Shape to Tune Domain Spacing in Block Copolymer Thin Films. *J. Am. Chem. Soc.* **2018,** *140*, 4639-4648.

25. Yadav, V.; Hashmi, N.; Ding, W.; Li, T.-H.; Mahanthappa, M. K.; Conrad, J. C.; Robertson, M. L. Dispersity Control in Atom Transfer Radical Polymerizations through Addition of Phenylhydrazine. *Polym. Chem.* **2018,** *9*, 4332-4342.

26. Ouchi, M.; Terashima, T.; Sawamoto, M. Transition Metal-Catalyzed Living Radical Polymerization: Toward Perfection in Catalysis and Precision Polymer Synthesis. *Chem. Rev.* **2009,** *109*, 4963-5050.

27. Ruzette, A.-V.; Tencé-Girault, S.; Leibler, L.; Chauvin, F.; Bertin, D.; Guerret, O.; Gérard, P. Molecular Disorder and Mesoscopic Order in Polydisperse Acrylic Block Copolymers Prepared by Controlled Radical Polymerization. *Macromolecules* **2006,** *39*, 5804-5814.

28. Bendejacq, D.; Ponsinet, V.; Joanicot, M.; Loo, Y. L.; Register, R. A. Well-Ordered Microdomain Structures in Polydisperse Poly(Styrene)–Poly(Acrylic Acid) Diblock Copolymers from Controlled Radical Polymerization. *Macromolecules* **2002,** *35*, 6645-6649.

29. Lynd, N. A.; Hillmyer, M. A. Effects of Polydispersity on the Order-Disorder Transition in Block Copolymer Melts. *Macromolecules* **2007,** *40*, 8050-8055.

30. Lynd, N. A.; Hamilton, B. D.; Hillmyer, M. A. The Role of Polydispersity in the Lamellar Mesophase of Model Diblock Copolymers. *J. Polym. Sci. Part B: Polym. Phys.* **2007,** *45*, 3386-3393.

31. Lynd, N. A.; Hillmyer, M. A. Influence of Polydispersity on the Self-Assembly of Diblock Copolymers. *Macromolecules* **2005,** *38*, 8803-8810.

32. Li, S.; Register, R. A.; Weinhold, J. D.; Landes, B. G. Melt and Solid-State Structures of Polydisperse Polyolefin Multiblock Copolymers. *Macromolecules* **2012,** *45*, 5773-5781.

33. Widin, J. M.; Schmitt, A. K.; Schmitt, A. L.; Im, K.; Mahanthappa, M. K. Unexpected Consequences of Block Polydispersity on the Self-Assembly of ABA Triblock Copolymers. *J. Am. Chem. Soc.* **2012,** *134*, 3834-3844.

34. Register, R. A. Continuity through Dispersity. *Nature* **2012,** *483*, 167-168.

35. Listak, J.; Jakubowski, W.; Mueller, L.; Plichta, A.; Matyjaszewski, K.; Bockstaller, M. R. Effect of Symmetry of Molecular Weight Distribution in Block Copolymers on Formation of "Metastable" Morphologies. *Macromolecules* **2008,** *41*, 5919-5927.

36. Lynd, N. A.; Hillmyer, M. A.; Matsen, M. W. Theory of Polydisperse Block Copolymer Melts: Beyond the Schulz-Zimm Distribution. *Macromolecules* **2008,** *41*, 4531-4533.

37. Schmitt, A. K.; Mahanthappa, M. K. Order and Disorder in High χ/Low N, Broad Dispersity ABA Triblock Polymers. *Macromolecules* **2017,** *50*, 6779-6787.

38. Schmitt, A. K.; Mahanthappa, M. K. Characteristics of Lamellar Mesophases in Strongly Segregated Broad Dispersity ABA Triblock Copolymers. *Macromolecules* **2014,** *47*, 4346-4356.

39. Schmitt, A. L.; Mahanthappa, M. K. Polydispersity-Driven Shift in the Lamellar Mesophase Composition Window of PEO-PB-PEO Triblock Copolymers. *Soft Matter* **2012,** *8*, 2294-2303.

40. Widin, J. M.; Schmitt, A. K.; Im, K.; Schmitt, A. L.; Mahanthappa, M. K. Polydispersity-Induced Stabilization of a Disordered Bicontinuous Morphology in ABA Triblock Copolymers. *Macromolecules* **2010,** *43*, 7913-7915.

41. Bates, C. M.; Bates, F. S. 50th Anniversary Perspective: Block Polymers-Pure Potential. *Macromolecules* **2017,** *50*, 3-22.

42. Hillmyer, M. A. Polydisperse Block Copolymers: Don't Throw Them Away. *J. Polym. Sci. Part B: Polym. Phys.* **2007,** *45*, 3249-3251.

43. Singh, M.; Odusanya, O.; Wilmes, G. M.; Eitouni, H. B.; Gomez, E. D.; Patel, A. J.; Chen, V. L.; Park, M. J.; Fragouli, P.; Iatrou, H.; Hadjichristidis, N.; Cookson, D.; Balsara, N. P. Effect of Molecular Weight on the Mechanical and Electrical Properties of Block Copolymer Electrolytes. *Macromolecules* **2007,** *40*, 4578-4585.

44. Teran, A. A.; Balsara, N. P. Thermodynamics of Block Copolymers with and without Salt. *J. Phys. Chem. B* **2014,** *118*, 4-17.

45. Loo, W. S.; Galluzzo, M. D.; Li, X.; Maslyn, J. A.; Oh, H. J.; Mongcopa, K. I.; Zhu, C.; Wang, A. A.; Wang, X.; Garetz, B. A.; Balsara, N. P. Phase Behavior of Mixtures of Block Copolymers and a Lithium Salt. *J. Phys. Chem. B* **2018,** *122*, 8065-8074.

46. Nakamura, I.; Balsara, N. P.; Wang, Z. G. Thermodynamics of Ion-Containing Polymer Blends and Block Copolymers. *Phys. Rev. Lett.* **2011,** *107*, 1-5.

47. Young, W. S.; Epps, T. H. Salt Doping in PEO-Containing Block Copolymers: Counterion and Concentration Effects. *Macromolecules* **2009,** *42*, 2672-2678.

48. Armarego, W. L. F.; Chai, C. L. L., *Purification of Laboratory Chemicals*. Butterworth-Heinemann: Waltham, MA, 2009.

49. Hayakawa, Y.; Kato, H.; Uchiyama, M.; Kajino, H.; Noyori, R. Allyloxycarbonyl Group: A Versatile Blocking Group for Nucleotide Synthesis. *J. Org. Chem.* **1985,** *51*, 2400-2402.

50. Lipscomb, C. E.; Mahanthappa, M. K. Microphase Separation Mode-Dependent Mechanical Response in Poly(Vinyl Ester)/PEO Triblock Copolymers. *Macromolecules* **2011,** *44*, 4401-4409.

51. Park, J. H.; Jeon, J. Y.; Lee, J. J.; Jang, Y.; Varghese, J. K.; Lee, B. Y. Preparation of High-Molecular-Weight Aliphatic Polycarbonates by Condensation Polymerization of Diols and Dimethyl Carbonate. *Macromolecules* **2013,** *46*, 3301-3308.

52. Mark, J. E., Physical Properties of Polymers Handbook. in 2 nd ed.; Mark, J. E., Ed. Springer: Philadelphia, PA, 2007.

53. Bates, F. S. Measurement of the Correlation Hole in Homogeneous Block Copolymer Melts. *Macromolecules* **1985,** *18*, 525-528.

54. Lee, I.; Panthani, T. R.; Bates, F. S. Sustainable Poly(Lactide-B-Butadiene) Multiblock Copolymers with Enhanced Mechanical Properties. *Macromolecules* **2013,** *46*, 7387-7398.

55. Gomez, E. D.; Panday, A.; Feng, E. H.; Chen, V.; Stone, G. M.; Minor, A. M.; Kisielowski, C.; Downing, K. H.; Borodin, O.; Smith, G. D.; Balsara, N. P. Effect of Ion Distribution on Conductivity of Block Copolymer Electrolytes. *Nano Lett.* **2009,** *9*, 1212-1216.

56. Likhtman, A. E.; Semenov, A. N. An Advance in the Theory of Strongly Segregated Polymers. *Europhys. Lett.* **2000,** *51*, 307-313.

57. Matsen, M. W.; Bates, F. S. Block Copolymer Microstructures in the Intermediate-Segregation Regime. *J. Chem. Phys.* **1997,** *106*, 2436-2448.

58. Yuan, R.; Teran, A. A.; Gurevitch, I.; Mullin, S. A.; Wanakule, N. S.; Balsara, N. P. Ionic Conductivity of Low Molecular Weight Block Copolymer Electrolytes. *Macromolecules* **2013,** *46*, 914-921.

59. Panday, A.; Mullin, S.; Gomez, E. D.; Wanakule, N.; Chen, V. L.; Hexemer, A.; Pople, J.; Balsara, N. P. Effect of Molecular Weight and Salt Concentration on Conductivity of Block Copolymer Electrolytes. *Macromolecules* **2009,** *42*, 4632-4637.

60. Thelen, J. L.; Teran, A. A.; Wang, X.; Garetz, B. A.; Nakamura, I.; Wang, Z. G.; Balsara, N. P. Phase Behavior of a Block Copolymer/Salt Mixture through the Order-to-Disorder Transition. *Macromolecules* **2014,** *47*, 2666-2673.

61. Nakamura, I.; Balsara, N. P.; Wang, Z. G. First-Order Disordered-to-Lamellar Phase Transition in Lithium Salt-Doped Block Copolymers. *ACS Macro Lett.* **2013,** *2*, 478-481.

62. Teran, A. A.; Mullin, S. A.; Hallinan, D. T.; Balsara, N. P. Discontinuous Changes in Ionic Conductivity of a Block Copolymer Electrolyte through an Order-Disorder Transition. *ACS Macro Lett.* **2012,** *1*, 305-309.

63. Matsen, M. W.; Thompson, R. B. Equilibrium Behavior of Symmetric ABA Triblock Copolymer Melts. *J. Chem. Phys.* **1999,** *111*, 7139-7146.

64. Medapuram, P.; Glaser, J.; Morse, D. C. Universal Phenomenology of Symmetric Diblock Copolymers Near the Order–Disorder Transition. *Macromolecules* **2015,** *48*, 819-839.

65. Matsen, M. W. Comparison of A-Block Polydispersity Effects on BAB Triblock and AB Diblock Copolymer Melts. *Eur. Phys. J. E* **2013,** *36*, 44 (41-47).

66. Pandav, G.; Ganesan, V. Fluctuation Effects on the Order-Disorder Transition in Polydisperse Copolymer Melts. *J. Chem. Phys.* **2013,** *139*, 214905.

67. Beardsley, T. M.; Matsen, M. W. Monte Carlo Phase Diagram for a Polydisperse Diblock Copolymer Melt. *Macromolecules* **2011,** *44*, 6209-6219.

68. Oschmann, B.; Lawrence, J.; Schulze, M. W.; Ren, J. M.; Anastasaki, A.; Luo, Y.; Nothling, M. D.; Pester, C. W.; Delaney, K. T.; Connal, L. A.; McGrath, A. J.; Clark, P. G.; Bates, C. M.; Hawker, C. J. Effects of Tailored Dispersity on the Self-Assembly of Dimethylsiloxane-Methyl Methacrylate Block Co-Oligomers. *ACS Macro Lett.* **2017,** *6*, 668-673.

69. Nakamura, I.; Wang, Z. G. Salt-Doped Block Copolymers: Ion Distribution, Domain Spacing and Effective χ Parameter. *Soft Matter* **2012,** *8*, 9356-9367.

70. Wang, Z. G. Effects of Ion Solvation on the Miscibility of Binary Polymer Blends. *J. Phys. Chem. B* **2008,** *112*, 16205-16213.

71. Borodin, O.; Smith, G. D. Mechanism of Ion Transport in Amorphous Poly(Ethylene Oxide)/LiTFSI from Molecular Dynamics Simulations. *Macromolecules* **2006,** *39*, 1620-1629.

72. Mao, G.; Saboungi, M. L.; Price, D. L.; Armand, M. B.; Howells, W. S. Structure of Liquid PEO-LiTFSI Electrolyte. *Phys. Rev. Lett.* **2000,** *84*, 5536-5539.

73. Borodin, O.; Smith, G. D. Molecular Dynamics Simulations of Poly(Ethylene Oxide)/Li Melts. 1. Structural and Conformational Properties. *Macromolecules* **1998,** *31*, 8396-8406.

74. Ren, C. L.; Nakamura, I.; Wang, Z. G. Effects of Ion-Induced Cross-Linking on the Phase Behavior in Salt-Doped Polymer Blends. *Macromolecules* **2016,** *49*, 425-431.

75. Xie, S.; Lodge, T. P. Phase Behavior of Binary Polymer Blends Doped with Salt. *Macromolecules* **2018,** *51*, 266-274.